The phonon-induced line shape of the dynamical Stark effect in Cu_2O

1992 J. Phys.: Condens. Matter 4 121

(http://iopscience.iop.org/0953-8984/4/1/022)

J. Phys.: Condens. Matter 4 (1992) 121–133. Printed in the UK

The phonon-induced line shape of the dynamical Stark effect in Cu_2O

J Schlösser†, Ch Neumann‡ and A Stahl†

† Institut für Theoretische Physik, RWTH Aachen, D-5100 Aachen, Federal Republic of Germany

‡ Institut für Physik, Universität Dortmund, D-4600 Dortmund 50, Federal Republic of Germany

Received 25 July 1991

Abstract. We study the influence of electron–phonon coupling on the resonant dynamical Stark effect in Cu_2O. We start from a multi-band density matrix theory involving directly forbidden dipole transitions and directly allowed quadrupole transitions. The use of the multi-band formalism is necessary for the inclusion of the observed polarization effects. From a microscopic treatment of the electron–phonon interaction we derive a frequency-dependent transverse relaxation for the excitons and a renormalization of the optical transition matrix elements resulting in a Fano effect. We derive an expression for the differential transmission, taking into account a parametric sum frequency generation. Theoretical and experimental data are compared, showing satisfactory agreement.

1. Introduction

The optical Stark effect of excitons in semiconductors consists in a modification of the excitonic absorption induced by a strong pump beam in the transparent spectral region. Since the first observation of the dynamical 'resonant' intraband Stark effect in a semiconductor by Fröhlich *et al* [1] a large variety of further experimental and theoretical studies have been performed. By contrast to the *resonant* intraband Stark effect, a '*non-resonant*' interband Stark effect was observed by Mysyrowicz *et al* [2] and Von Lehmen *et al* [3] in GaAs quantum wells and by Joffre *et al* [4] in a GaAs bulk semiconductor.

Density matrix theory [5–10] has been developed into a powerful tool for use in the investigation of the dynamics of electronic processes in semiconductors and especially the various manifestations of the Stark effect. Density matrix methods described in the literature [7, 11–14] usually introduce longitudinal (τ_1) and transverse (τ_2) relaxation times phenomenologically. The transverse relaxation is much faster than recombination and plays a decisive role in the optical Stark effect. Detailed experimental and theoretical studies of the corresponding absorption line shapes during the last few years indicated limitations on the use of phenomenological damping constants in the density matrix theory [1, 12, 15, 16, 18]. These shortcomings can only be overcome by using a microscopic theory of damping.

Toyozawa [19, 20], Segall *et al* [21, 22] and Rudin *et al* [23, 24] studied the effect of lattice vibrations in linear exciton absorption spectra. Novel approaches [25–27] discuss a non-Markovian dephasing of the excitonic polarization in the interband Stark effect

0953-8984/92/010121 + 13 $03.50

due to exciton–phonon interaction. A conclusion that can be drawn from earlier work is that each non-linear optical effect has its own damping characteristics necessitating a special treatment. In the present paper we shall develop a density matrix approach to the dynamics of the intraband Stark effect in Cu_2O observed by Fröhlich *et al* [1, 16] with special emphasis on exciton–phonon interaction and selection rules.

In the experiment reported by Fröhlich *et al* [1] the 2p and 1s exciton were dynamically coupled by a strong infrared laser field (CO_2 laser) and the induced change in absorption was observed in the directly forbidden dipole transition to the 2p exciton tested by a weak laser beam (tunable dye laser). This experiment was explained within a three-level system, introducing a special phenomenological *ansatz* for the frequency-dependent transverse relaxation of the 2p exciton.

Another way to study the coupling to the 1s and 2p exciton caused by the pump field is to measure the induced absorption in the directly allowed quadrupole transition to the 1s exciton [16, 17]. Because the quadrupole absorption of the 1s exciton is two orders of magnitude smaller than the dipole absorption of the 2p exciton, in the experiment [16] a sample of 3 mm thickness was used instead of the 60 μm sample used in the former experiment [1]. As a consequence, the attenuation of the test beam due to sum frequency generation must be taken into account. It turns out that the strength of this effect is comparable to that of the quadrupole absorption. The results of this experiment could not be explained using the theoretical treatment mentioned above. The paper is organized as follows: in section 2 we shall first describe the experimental set-up that was used to study the Stark effect in Cu_2O. In section 3 we formulate the model and perform relevant projections based on exciton eigenfunctions. In section 4 an expression for the differential transmission will be derived. Comparisons between theory and experiment will be made in section 5. The calculated differential transmission spectra are in fair agreement with experimental findings.

2. Experimental set-up

The experiments on the quadrupole transition to the 1s exciton in Cu_2O were performed with a picosecond set-up, as shown in figure 1. Details of the active-mode-locked YAG dye laser system are given in [16]. The CO_2 laser pulse is synchronized to the 60 ps dye laser pulse by plasma switching. The 150 ns CO_2 laser pulse from a single-mode CO_2 laser is incident at the Brewster angle with perfect horizontal polarization on a germanium plate. The YAG pulse excites a plasma in the germanium plate which leads to an instantaneous rise of the reflectivity for the CO_2 pulse. The finite lifetime of the plasma yields rather long CO_2 pulses (250 ps). The suppression of the 150 ns CO_2 laser pulse was better than 1 : 500. The short pulse is further amplified in a TEA amplifier. The dye laser beam is focused to a waist of about 30 μm so as to overlap perfectly the waist of the CO_2 laser—about 90 μm. Both pump and probe beam are directed on the sample with nearly normal incidence and the same linear polarization.

3. The model

The starting point will be the real-space representation of the electron–hole density matrix theory [10]. The point group of Cu_2O is O_h and the band structure is given in [28]. Because of the experimental situation, only the twofold-degenerate Γ_7^+ valence band

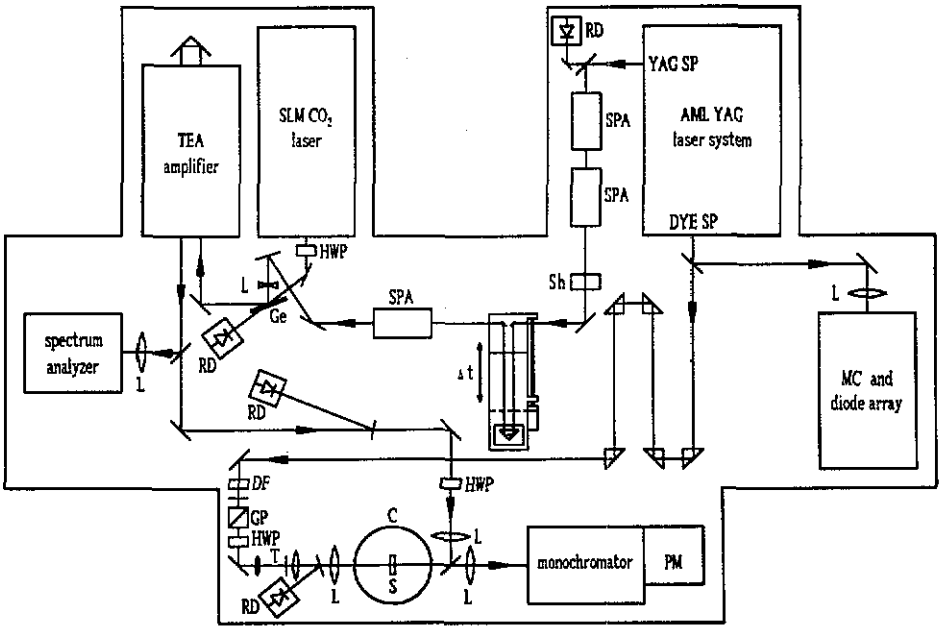

Figure 1. Experimental set-up.

and the Γ_6^+ conduction band need to be considered. As pointed out previously, the strong infrared pump beam is resonant with the 1s–2p transition. Following arguments given in [12] and [14], no populations are produced in this case by the pump field, and only the interband transition submatrix **Y** of the complete density matrix is active. The transition matrix **Y** is driven by the electric multipole sources [8, 29]. Because of the large exciton mass, we can neglect the centre-of-mass motion. The equations of motion then take the form

$$(i\hbar\,\partial/\partial t + \hbar\Omega)Y_{vc}(\boldsymbol{r},\boldsymbol{R},t) = (\boldsymbol{M}_{cv}(\boldsymbol{r}) + \nabla_R Q_{cv}(\boldsymbol{r}))\boldsymbol{E}^{t}(\boldsymbol{R},t)$$
$$-e\boldsymbol{r}\cdot\boldsymbol{E}^{p}(\boldsymbol{R},t)Y_{vc}(\boldsymbol{r},\boldsymbol{R},t) + (\Sigma Y_{vc})(\boldsymbol{r},\boldsymbol{R},t). \tag{1}$$

$\boldsymbol{r}, \boldsymbol{R}$ are the relative and centre-of-mass coordinates, respectively. The indices $v = 1, 2$ ($c = 1, 2$) are used to specify the total angular momentum quantum numbers of the Bloch functions of the Γ_7^+ valence (Γ_6^+ conduction) band at $k = 0$. The propagation operator $\hbar\Omega$ describes the propagation in configuration space:

$$\hbar\Omega = \hbar\omega_g - (\hbar^2/2\mu)\Delta_r - v(r). \tag{2}$$

μ is the reduced mass, $v(r)$ the Coulomb potential and $\hbar\omega_g$ the gap energy. The first term on the RHS of (1) describes the linear excitation from the ground state via radiative dipole ($\boldsymbol{M}$) and quadrupole ($\boldsymbol{Q}$) transitions induced by the weak test beam $\boldsymbol{E}^{t}$. The dipole and quadrupole transition densities are given by

$$\boldsymbol{M}_{cv}(r) := \frac{-e}{(2\pi)^3}\int_{1\,BZ} d^3k\, e^{ik\cdot r}\langle\psi_{k,c}|\boldsymbol{r}|\psi_{k,v}\rangle \tag{3}$$

$$Q_{cv}(r) := \frac{-e}{2(2\pi)^3}\int_{1\,BZ} d^3k\, e^{ik\cdot r}\langle\psi_{k,c}|\boldsymbol{r}\otimes\boldsymbol{r}|\psi_{k,v}\rangle \tag{4}$$

where 1BZ ≡ first Brillouin zone. For excitations near the zone centre it is useful to expand the Bloch functions in the above expressions around $\boldsymbol{k} = 0$ and retain the first non-vanishing moments. Both the valence band and the conduction band have positive parity at $\boldsymbol{k} = 0$; this yields

$$\boldsymbol{M}_{cv}(\boldsymbol{r}) \simeq -\boldsymbol{M}_{1cv}\nabla_r\delta(\boldsymbol{r}). \tag{5}$$

Thus the directly forbidden dipole transition acts as a p-symmetric point-like source for p-like excitations in relative space in (1). The second-rank matrix with elements $\boldsymbol{M}_{1cv}$ can be obtained by $\boldsymbol{k}\cdot\boldsymbol{p}$ perturbation theory [30]. In contrast the quadrupole transitions are directly allowed:

$$\boldsymbol{Q}_{cv}(\boldsymbol{r}) = \boldsymbol{Q}_{0cv}\delta(\boldsymbol{r}). \tag{6}$$

This gives rise to an s-symmetric point-like source in relative space driving s-like excitations. The second-rank matrices with elements $\boldsymbol{M}_{1cv}$ and $\boldsymbol{Q}_{0cv}$ contain both the coupling strength and the selection rules. The second term on the RHS of (1) leads to the coupling between excitons of different parity caused by the strong pump field $\boldsymbol{E}^{\mathrm{P}}$. The last term on the RHS of (1) is a consequence of the electron–phonon interaction and takes into account the propagation of the transition density $\mathbf{Y}$ in an incoherent thermal phonon environment. Σ is the phonon self-energy operator; it will be calculated by a method that is a refined version of the approach used in [31]. The explicit form of this term will be discussed later. The macroscopic polarization $\boldsymbol{P}(\boldsymbol{R}, t)$ comprises all possible dipole and quadrupole contributions:

$$\boldsymbol{P}(\boldsymbol{R}, t) = \sum_{vc} 2\mathrm{Re}\left(\int \mathrm{d}^3r\,(\boldsymbol{M}^*_{cv}(\boldsymbol{r}) - (\boldsymbol{Q}^*_{cv}(\boldsymbol{r})\nabla_R))Y_{vc}(\boldsymbol{r}, \boldsymbol{R}, t)\right). \tag{7}$$

Expanding $\mathbf{Y}$ in terms of excitonic eigenfunctions $\varphi_l(\boldsymbol{r})$

$$Y_{vc}(\boldsymbol{r}, \boldsymbol{R}, t) = \sum_l \varphi_l(\boldsymbol{r})\,y_{lvc}(\boldsymbol{R}, t) \tag{8}$$

$$[-(\hbar^2/2\mu)\Delta_r - v(\boldsymbol{r})]\varphi_l(\boldsymbol{r}) = \mathscr{E}_l\varphi_l(\boldsymbol{r}) \tag{9}$$

we obtain, with the help of (5) and (6),

$$\boldsymbol{P}(\boldsymbol{R}, t) = \sum_{lvc} 2\mathrm{Re}[(\boldsymbol{M}^*_{1cv}\nabla_r\varphi_l(\boldsymbol{r})|_{r=0} - (\boldsymbol{Q}^*_{0cv}\nabla_R)^{\mathrm{t}}\varphi_l(0))\,y_{lvc}(\boldsymbol{R}, t)]. \tag{10}$$

It can be seen easily that the directly forbidden dipole transition 'reads' only the information contained in the p-symmetric expansion coefficients y_{pvc}, whereas the directly allowed quadrupole transition utilizes only the s-symmetric expansion coefficients y_{svc}.

Inserting the *ansatz* (8) in (1) and applying a Fourier transformation in time, one obtains equations for the coefficients $y_{lvc}(\boldsymbol{R}, \omega)$:

$$\Lambda^l(\omega)y_{lvc}(\boldsymbol{R}, \omega) = F_{lvc}(\boldsymbol{R}, \omega) + \sum_{l'} \boldsymbol{m}^{ll'}[\boldsymbol{E}^{\mathrm{P}} * y_{l'vc}](\boldsymbol{R}, \omega) + \sum_{l'} \Sigma^{ll'}(\omega)y_{l'vc}(\boldsymbol{R}, \omega) \tag{11}$$

with

$$F_{lvc}(\boldsymbol{R}, \omega) := \boldsymbol{M}_{1cv}\nabla_r\varphi^*_l(\boldsymbol{r})|_{r=0} + \nabla_R\boldsymbol{Q}_{0cv}\varphi^*_l(0)\boldsymbol{E}^{\mathrm{t}}(\boldsymbol{R}, \omega) \tag{12}$$

$$\Lambda^l(\omega) := \hbar\omega_{\mathrm{g}} + \mathscr{E}_l - \hbar\omega \tag{13}$$

$$\boldsymbol{m}^{ll'} := -e \int \mathrm{d}^3\boldsymbol{r}\, \varphi_l^*(\boldsymbol{r}) \boldsymbol{r} \varphi_{l'}(\boldsymbol{r}) \tag{14}$$

$$[\boldsymbol{E}^{\mathrm{p}} * y_{l'vc}](\boldsymbol{R}, \omega) := \frac{1}{2\pi} \int \mathrm{d}\xi\, \boldsymbol{E}^{\mathrm{p}}(\boldsymbol{R}, \omega - \xi) y_{l'vc}(\boldsymbol{R}, \xi). \tag{15}$$

Turning to the phonons in Cu_2O we note that besides the Γ_4^- acoustic mode there exist six optical modes belonging to representations Γ_5^-, Γ_5^+, $2\Gamma_4^-$, Γ_3^- and Γ_2^- [32]. As the experiment was performed at a temperature of 25 K we can assume that for the optical scattering only 'Stokes' transitions are relevant. Therefore the LA deformation potential scattering should be responsible for the damping of the 1s exciton [19]. The two Γ_4^- phonons are infrared active and may be expected to play the dominant role for the damping of the p-symmetric excitons because of their polar character [33]. Thus we restrict ourselves to taking into account only contributions from the Γ_4^- LA phonon and the two Γ_4^- LO phonons to the phonon self-energy. The phonon-induced electronic self-energy Σ is derived from the following integral equation:

$$\Sigma^{ll'}(\omega) = \Sigma^{ll'}_{\mathrm{LA}}(\omega) + \sum_{\lambda_{\mathrm{LO}}} \Sigma^{ll'}_{\lambda_{\mathrm{LO}}}(\omega) \tag{16}$$

with

$$\Sigma^{ll'}_{\mathrm{LA}}(\omega) := \sum_{\pm} \sum_{q} \sum_{l''} \frac{\hbar q}{2V\rho c_{\mathrm{LA}}} \left\{ \left[\exp\left(\frac{\hbar q c_{\mathrm{LA}}}{k_{\mathrm{B}} T} \right) - 1 \right]^{-1} + 1/2 \mp 1/2 \right\}$$
$$\times \frac{(d_{\mathrm{e}} \cdot s_{\mathrm{e}}(\boldsymbol{q}, ll'') - d_{\mathrm{h}} \cdot s_{\mathrm{h}}(\boldsymbol{q}, ll''))(d_{\mathrm{e}} \cdot s_{\mathrm{e}}^*(\boldsymbol{q}, l'l'') - d_{\mathrm{h}} \cdot s_{\mathrm{h}}^*(\boldsymbol{q}, l'l''))}{\hbar\omega_{\mathrm{g}} + \mathscr{E}_{l''} + \hbar^2 q^2/2M - \hbar(\omega + \mathrm{i}\eta \pm q c_{\mathrm{LA}}) - \Sigma^{l''l''}(\omega \pm q c_{\mathrm{LA}})} \tag{17}$$

as $\eta \to 0^+$. d_{e} and d_{h} are the acoustical deformation potentials of the Γ_6^+ conduction band and the Γ_7^+ valence band. ρ is the density of Cu_2O, V the crystal volume, c_{LA} the longitudinal sound velocity and M the exciton mass.

In the limit of low temperatures we neglect the thermal occupation of the optical phonons; this yields

$$\Sigma^{ll'}_{\lambda_{\mathrm{LO}}}(\omega) := \sum_{q} \sum_{l''} \frac{1}{q^2} \frac{\hbar e^2}{V\varepsilon_0} \left(\frac{\partial}{\partial \omega} \varepsilon_{\parallel}(\omega)\big|_{\omega = \omega_{\lambda_{\mathrm{LO}}}} \right)^{-1}$$
$$\times \frac{(s_{\mathrm{e}}(\boldsymbol{q}, ll'') - s_{\mathrm{h}}(\boldsymbol{q}, ll''))(s_{\mathrm{e}}^*(\boldsymbol{q}, l'l'') - s_{\mathrm{h}}^*(\boldsymbol{q}, l'l''))}{\hbar\omega_{\mathrm{g}} + \mathscr{E}_{l''} + \hbar^2 q^2/2M - \hbar(\omega + \mathrm{i}\eta - \omega_{\lambda_{\mathrm{LO}}}) - \Sigma^{l''l''}(\omega - \omega_{\lambda_{\mathrm{LO}}})} \tag{18}$$

as $\eta \to 0^+$. The Fröhlich coupling constants in (18) are derived from the LST relation in the limit $\boldsymbol{q} \to 0$ [34]:

$$\frac{\varepsilon_{\parallel}(\omega)}{\varepsilon(\infty)} = \frac{\omega^2 - \omega_{\mathrm{LO1}}^2}{\omega^2 - \omega_{\mathrm{TO1}}^2} \cdot \frac{\omega^2 - \omega_{\mathrm{LO2}}^2}{\omega^2 - \omega_{\mathrm{TO2}}^2}. \tag{19}$$

The structure functions $s_{\mathrm{e}}(\boldsymbol{q}, ll')$ and $s_{\mathrm{h}}(\boldsymbol{q}, ll')$ are defined as follows:

$$s_{\mathrm{e}}(\boldsymbol{q}, ll') = \int \mathrm{d}^3\boldsymbol{r}\, \varphi_l^*(\boldsymbol{r})\, \mathrm{e}^{\mathrm{i}\beta\boldsymbol{q}\cdot\boldsymbol{r}}\, \varphi_{l'}(\boldsymbol{r}) \tag{20}$$

$$s_{\mathrm{h}}(\boldsymbol{q}, ll') = \int \mathrm{d}^3\boldsymbol{r}\, \varphi_l^*(\boldsymbol{r})\, \mathrm{e}^{-\mathrm{i}\alpha\boldsymbol{q}\cdot\boldsymbol{r}}\, \varphi_{l'}(\boldsymbol{r}) \tag{21}$$

$$\alpha = m_e/M \qquad \beta = m_h/M. \tag{22}$$

In general the expressions for Σ_{LA} and $\Sigma_{\lambda_{LO}}$ cannot be evaluated separately because they are coupled by Σ in the energy denominators in (17) and (18). The frequency dependence of Σ determines the phase memory.

Note that we have only considered scattering by spontaneous phonon distributions. Stimulated phonons will not be present because their source terms would be real carrier densities derived from the intraband density matrices **C** and **D**. These quantities are not activated in the intraband Stark effect since this effect consists in a coherent oscillation between different envelopes of the transition density **Y**.

4. A simplified expression for the differential transmission

The task of finding a solution of (11) explaining the measurements given in [16] is considerably simplified by the following:

(i) the energetic splitting between the 1s and 2p excitons is 115 meV; this is very close to the value for the CO_2 laser lines used in the experiment and larger than any phonon energy in Cu_2O;

(ii) the ns exciton resonances, $n > 1$, lie at least 115 meV above the 1s exciton resonances;

(iii) the energetic splitting of the 2p and np excitons, $n > 2$, is larger than 13 meV;

(iv) with the neglect of centre-of-mass motion, the matrix elements of the phonon self-energy $\Sigma^{ll'}$ vanish if l, l' belong to different irreducible representations of the excitonic states [20].

From the first point it follows that the broadening of the 1s exciton is due to the deformation potential scattering and only the 1s exciton in the internal summation over exciton states in Σ_{LA} is important. Taking this together with the second point, it follows that one has only to deal with the 1s exciton, rather than the whole s series. Using properties (i), (ii) and (iv) the matrix equation (11) can be reduced to a system for the expansion coefficients of the 1s exciton and the p exciton series. In the following we shall suppress the arguments $\boldsymbol{R}$, ω and the band indices v, c. For the threefold-degenerate p excitons we choose a symmetric vector representation $\boldsymbol{y}_p := (y_{p_x}, y_{p_y}, y_{p_z})$ with respect to the principal axes of the crystal. The relevant set of equations is then given by

$$(\Lambda^{1s} - \Sigma^{1s1s})y_{1s} = F_{1s} + m^{1s2p}[\boldsymbol{E}^p * \boldsymbol{y}_{2p}] + \sum_n m^{1sn}[\boldsymbol{E}^p * \boldsymbol{y}_n] \tag{23}$$

$$(\Lambda^{2p} - \Sigma^{2p2p})\boldsymbol{y}_{2p} = \boldsymbol{F}_{2p} + m^{2p1s}[\boldsymbol{E}^p * y_{1s}] + \sum_n \Sigma^{2pn}\boldsymbol{y}_n \tag{24}$$

$$\Lambda^n \boldsymbol{y}_n = \boldsymbol{F}_n + m^{n1s}[\boldsymbol{E}^p * y_{1s}] + \sum_{n'} \Sigma^{nn'}\boldsymbol{y}_{n'} + \Sigma^{n2p}\boldsymbol{y}_{2p} \tag{25}$$

with

$$F_{svc}(\boldsymbol{R}, \omega) = \varphi_s^*(0)\nabla_{\boldsymbol{R}}\boldsymbol{Q}_{0cv}\boldsymbol{E}^t(\boldsymbol{R}, \omega) \tag{26}$$

$$\boldsymbol{F}_{p_jvc}(\boldsymbol{R}, \omega) = \varphi'^*_{pz}(0)\boldsymbol{E}^t(\boldsymbol{R}, \omega)\boldsymbol{M}_{1cv}\hat{\boldsymbol{e}}_j \qquad j = x, y, z \tag{27}$$

and

$$m^{sp} := -e\int \mathrm{d}^3\boldsymbol{r}\,\varphi_s^*(\boldsymbol{r})z\varphi_{p_z}(\boldsymbol{r}) = m^{ps*}. \tag{28}$$

Indices n, n', ... denote the np excitons ($n, n', \ldots > 2$) and $\hat{\boldsymbol{e}}_j$ ($j = x, y, z$) are unit

vectors in the direction of the principal axes. For the calculation of the phonon self-energy $\Sigma^{pp'}$ the exciton wave functions φ_{p_z} and $\varphi_{p_z'}$ have to be inserted. The equations are valid for both, testing the 1s quadrupole absorption (illustrated in figure 2) or the 2p dipole absorption.

The pump-induced coupling between the 1s and the 2p exciton has to be treated in infinite order in the pump field $\boldsymbol{E}^p$, whereas for the np excitons, $n > 2$, a calculation up to third order in the electric field is assumed sufficient (first order in test beam and second order in pump field). The np excitons are energetically well separated from the 2p exciton (point (iii) of the above comments), so one expects that only one-phonon-assisted contributions to the absorption of the 2p exciton are relevant. Thus (23)–(25) take on the form

$$\Xi^{1s} y_{1s} = F_{1s} + |m^{1s2p}|^2 [\boldsymbol{E}^p * (g^{1s}[\boldsymbol{E}^p * y_{1s}])] + [\boldsymbol{E}^p * (m^{1s2p}(1 + B^{1s2p}) y_{2p})] \tag{29}$$

$$\Xi^{2p} y_{2p} = F_p(1 + A1^{2p}) + m^{2p1s}(1 + B^{2p1s})[\boldsymbol{E}^p * y_{1s}] \tag{30}$$

$$\Lambda^n y_n = F_n(1 + A1^n) + \Sigma^{n2p} y_{2p} \tag{31}$$

with

$$\Xi^{1s} := \Lambda^{1s}(\omega) - \Sigma^{1s1s}(\omega) \tag{32}$$

$$\Xi^{2p} := \Lambda^{2p}(\omega) - \Sigma^{2p2p}(\omega) \tag{33}$$

and

$$g^{1s}(\omega) := \frac{1}{|m^{1s2p}|^2} \left(\sum_n \frac{|m^{1sn}|^2}{\Lambda^n(\omega)} + \sum_{nn'} \frac{m^{1sn} \Sigma^{nn'}(\omega) m^{n'1s}}{\Lambda^n(\omega) \Lambda^{n'}(\omega)} \right) \tag{34}$$

$$B^{sp}(\omega) := \frac{1}{|m^{sp}|^2} \sum_n \frac{m^{sn} \Sigma^{np}(\omega) m^{ps}}{\Lambda^n(\omega)} \tag{35}$$

$$B^{ps}(\omega) := \frac{1}{|m^{sp}|^2} \sum_n \frac{m^{sp} \Sigma^{pn}(\omega) m^{ns}}{\Lambda^n(\omega)} \tag{36}$$

$$A1^p(\omega) := \frac{1}{|\varphi'_{p_z}(0)|^2} \sum_n \frac{\varphi'_{p_z}(0) \Sigma^{pn}(\omega) \varphi'^*_{n_z}(0)}{\Lambda^n(\omega)}. \tag{37}$$

Assuming a quasi-monochromatic pump field with frequency ω_p, one obtains for the case

$$\hbar\omega \simeq \hbar\omega_g + \mathscr{E}_{1s} - \mathrm{Re}\{\Sigma^{1s1s}\} \tag{38}$$

$$y_{1s}(\omega) = \left(\tilde{\Xi}^{1s}(\omega) - \frac{|m^{1s2p}|^2 |\boldsymbol{E}^p|^2 b^{1s2p}(\omega + \omega_p)}{\Xi^{2p}(\omega + \omega_p)} \right)^{-1} F_{1s}(\omega) \tag{39}$$

with

$$\tilde{\Xi}^{1s}(\omega) := \Xi^{1s}(\omega) - |m^{1s2p}|^2 |\boldsymbol{E}^p|^2 \sum_{\pm} g^{1s}(\omega \pm \omega_p) \tag{40}$$

$$b^{sp}(\omega) := (1 + B^{sp}(\omega))(1 + B^{ps}(\omega)). \tag{41}$$

The electron–phonon interaction leads to renormalization and damping of the 1s and 2p excitons ($\Lambda^{1s} \rightarrow \Xi^{1s} = \Lambda^{1s} - \Sigma^{1s1s}$, $\Lambda^{2p} \rightarrow \Xi^{2p} = \Lambda^{2p} - \Sigma^{2p2p}$). In addition, 'vertex' corrections of the envelope matrix elements ($m^{1s2p} \rightarrow m^{1s2p}(1 + B^{1s2p})$) are found. This is a

consequence of the pump-field-induced interaction with asymmetric p resonances. For the case $\hbar\omega \simeq \hbar\omega_g + \mathscr{E}_{2p} - \mathrm{Re}\{\Sigma^{2p2p}\}$, relevant for the situation where the probe is tuned to the 2p exciton, an analogous calculation [35] leads to results very similar to those reported earlier by Higashimura *et al* [36].

Inserting expression (39) into (10), the dielectric polarization $\boldsymbol{P}_{1s}(\boldsymbol{R}, \omega)$ of the 1s exciton becomes

$$\boldsymbol{P}_{1s}(\boldsymbol{R}, \omega) = |Q_0|^2 |\varphi_{1s}(0)|^2 \mathbf{T}(-\nabla_R, \nabla_R)\boldsymbol{E}^t(\boldsymbol{R}, \omega)$$
$$\times \left(\tilde{\Xi}^{1s}(\omega) - \frac{|m^{1s2p}|^2 |\boldsymbol{E}^p|^2 \cdot b^{1s2p}(\omega + \omega_p)}{\Xi^{2p}(\omega + \omega_p)}\right)^{-1} \tag{42}$$
$$:= \varepsilon_0 \chi_{1s}([\boldsymbol{E}^p], \omega)\boldsymbol{E}^t. \tag{43}$$

$|Q_0|^2$ is the strength of the quadrupole coupling. The coupling coefficients contained in Q_{0cv} are taken from Koster *et al* [37]. Performing the summation over v, c in (10) one obtains the 3×3 matrix $\mathbf{T}(\boldsymbol{L}, \boldsymbol{N})$, built up from the vector components of the vectors $\boldsymbol{L} = (L_x, L_y, L_z)$, $\boldsymbol{N} = (N_x, N_y, N_z)$ along the principal axes of Cu_2O as follows:

$$\mathbf{T}(\boldsymbol{L}, \boldsymbol{N}) := \begin{pmatrix} L_yN_y + L_zN_z & L_yN_x & L_zN_x \\ L_xN_y & L_xN_x + L_zN_z & L_zN_y \\ L_xN_z & L_yN_z & L_xN_x + L_yN_y \end{pmatrix}. \tag{44}$$

Therefore the matrix $\mathbf{T}(-\nabla_R, \nabla_R)$ describes the dependence of the dielectric polarization $\boldsymbol{P}_{1s}(\boldsymbol{R}, \omega)$ on the direction and the spatial inhomogeneity of the test field $\boldsymbol{E}^t(\boldsymbol{R}, \omega)$. The well known form of the selection rules for the quadrupole transition appears if one assumes $\boldsymbol{E}^t \sim \exp(i\boldsymbol{K} \cdot \boldsymbol{R})$.

The differential transmission is defined by $D := \ln(T_0/T)$, where T_0 is the linear transmission and T is the transmission in the presence of the pump beam. As in this system quadrupole and dipole transition densities are active (see figure 2), a sum frequency signal on the 2p resonance will be emitted. The corresponding polarization $\boldsymbol{P}_{sum}(\boldsymbol{R}, \omega + \omega_p)$ takes on the form

$$\boldsymbol{P}_{sum}(\boldsymbol{R}, \omega + \omega_p) = Q_0 \varphi^*_{1s}(0)\mathbf{T}(\boldsymbol{E}^p, \nabla_R)\boldsymbol{E}^t(\boldsymbol{R}, \omega)$$
$$\times m^{2p1s}(1 + B^{2p1s}(\omega + \omega_p))M_1^* \varphi'_{2p_z}(0)(1 + A2^{2p}(\omega + \omega_p))$$
$$\times (\tilde{\Xi}^{1s}(\omega)\Xi^{2p}(\omega + \omega_p) - |m^{1s2p}|^2 |\boldsymbol{E}^p|^2 b^{1s2p}(\omega + \omega_p))^{-1} \tag{45}$$
$$:= \varepsilon_0 \chi_{sum}([\boldsymbol{E}^p], \omega)\boldsymbol{E}^t \tag{46}$$

with

$$A2^p(\omega) := \frac{1}{|\varphi'_{p_z}(0)|^2} \sum_n \frac{\varphi'_{n_z}(0)\Sigma^{np}(\omega)\varphi'^*_{p_z}(0)}{\Lambda^n(\omega)}. \tag{47}$$

Thus the generation of the sum frequency depends on the directions of the test beam *and* the pump beam and also on the spatial inhomogeneity of the test field. $M_1^* \varphi'_{2p_z}(0)(1 + A2^{2p})$ is the strength of the directly forbidden dipole coupling to the 2p exciton with the 'vertex' correction due to the electron–phonon interaction. As the damping of the 2p resonance is two orders of magnitude larger than that of the 1s resonance one can assume that the whole power absorption $L_{sum}(\omega_s) = -\varepsilon_0\omega_s \,\mathrm{Im}\{\boldsymbol{E}^{s*}\chi_{sum}([\boldsymbol{E}^p], \omega)\boldsymbol{E}^t\}$ acts as an additional loss for the test beam [38, 39]

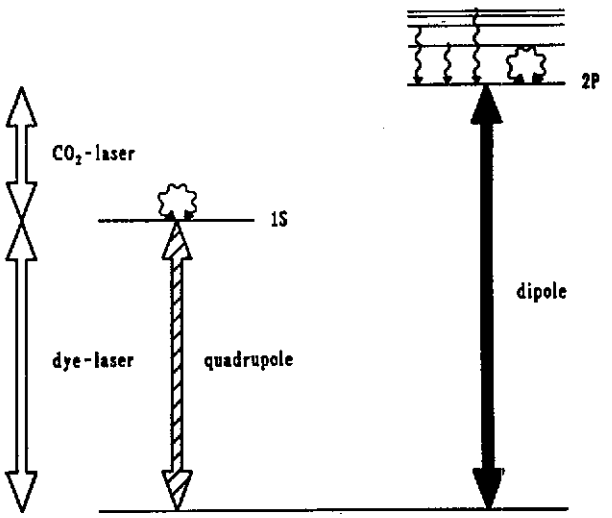

Figure 2. Level diagram for the quadrupole intraband Stark effect in Cu_2O. Only the coefficients y_{1s} of the quadrupole transition and the coefficients of the dipole transitions are active. Phonons are indicated by wavy arrows. The two-phonon loops are associated with phonon self-energies Σ^{1s1s} and Σ^{2p2p} and describe frequency-dependent renormalization and damping of the 1s and 2p exciton. The np excitons, $n > 2$, contribute via phonon-assisted processes.

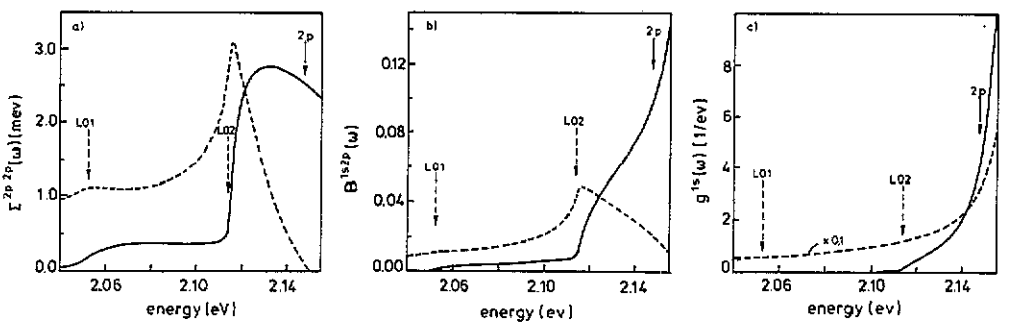

Figure 3. The calculated frequency-dependent quantities (a) $\Sigma^{2p2p}(\omega)$, (b) $B^{1s2p}(\omega)$ and (c) $g^{1s}(\omega)$. Dashed lines are real parts and solid lines imaginary parts. The spectral position of the measured energy of the 2p resonance is indicated by the full arrow whereas broken arrows denote the start of polar optical scattering due to the LO1 and LO2 phonons. The parameters used are given in table 1.

($\boldsymbol{E}^s$, $\omega_s = \omega + \omega_p$, is the generated sum frequency field). The selection rules are fulfilled in the experiment [16] and we get the following expression for the intensity I_{1s} of the test field:

$$\frac{\partial}{\partial x} I_{1s} = -\frac{f_{1s}}{d} \operatorname{Im}\left[\left(\tilde{\Xi}^{1s}(\omega) - \frac{|m^{1s2p}|^2 |E^p|^2 b^{1s2p}(\omega + \omega_p)}{\Xi^{2p}(\omega + \omega_p)}\right)^{-1}\right] \cdot I_{1s}$$

$$- \frac{f_{1s} \cdot f_{sum}}{d} |m^{1s2p}|^2 |E^p|^2 (1 + B^{2p1s}(\omega + \omega_p))(1 + A2^{2p}(\omega + \omega_p))$$

$$\times (\tilde{\Xi}^{1s}(\omega)\Xi^{2p}(\omega + \omega_p) - |m^{1s2p}|^2 |E^p|^2 \cdot b^{1s2p}(\omega + \omega_p))^{-1}|^2 \cdot I_{1s}. \quad (48)$$

Table 1. Parameters used in the calculations. m_0 is the bare electron mass. The parameters were taken from [28] and [40–42].

Parameter	Value
m_e	$0.98m_0$
m_h	$0.58m_0$
M	$1.56m_0$
$\hbar\omega_g$	2.1725 eV
Ryd $= \hbar^2/2\mu a_b^2$	0.09822 eV
a_b	1.034 nm
ρ	6.1×10^3 kg m^{-3}
c_{LA}	4.54×10^3 m s^{-1}
$\varepsilon(\infty)$	7.5
$\hbar\omega_{TO1}$	18.8 meV
$\hbar\omega_{LO1}$	19.1 meV
$\hbar\omega_{TO2}$	78.5 meV
$\hbar\omega_{LO2}$	82.1 meV

$d = 3$ mm is the thickness of the crystal. The prefactor f_{1s} is determined by a fit to the linear spectra, whereas f_{sum} is found from a fit to the non-linear spectra. At the temperature of 25 K the 1s exciton state in the internal summation in the expression (16) for the phonon self-energy is assumed to give the main contribution. Within the

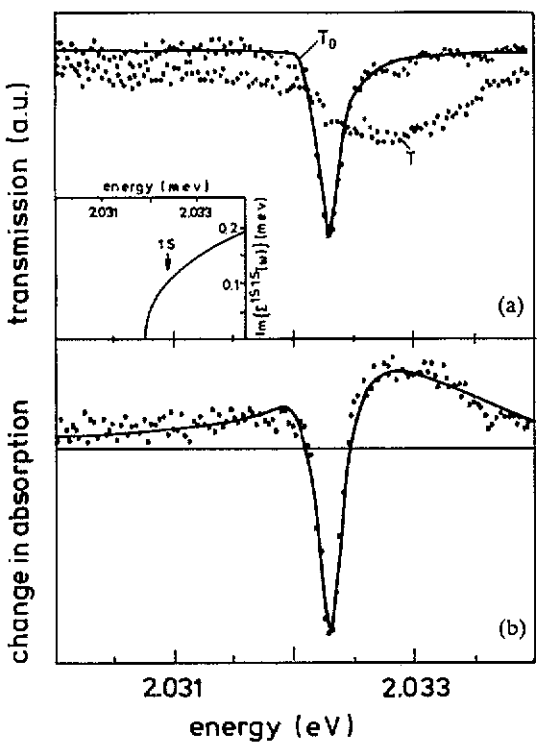

Figure 4. Comparison between experiment (dots) and theory (solid lines). (a) Original spectra: $T_0 \triangleq$ transmission without pump pulse and $T \triangleq$ transmission with pump beam. The inset shows the frequency-dependent damping of the 1s exciton ($\mathrm{Im}\{\Sigma^{1s1s}(\omega)\}$) due to LA phonon scattering with deformation potentials $d_e = 21$ eV and $d_h = 10.5$ eV. (b) Difference spectrum ($\hbar\omega_p = 116.8$ meV and $|m^{1s2p}|^2|E^p(0, \omega_p)|^2 = (2.8\ \mathrm{meV})^2$).

framework of the approximations applied we have calculated the quantities $\Sigma^{1s1s}(\omega)$, $\Sigma^{2p2p}(\omega)$, $B^{1s2p}(\omega) = B^{2p1s}(\omega)$ and $g^{1s}(\omega)$ numerically. In general these quantities are strongly dependent on frequency, but in the small energy interval measured experimentally the quantities $\Sigma^{2p2p}(\omega)$, $B^{1s2p}(\omega)$, $g^{1s}(\omega)$ and $A2^{2p}(\omega)$ depend only weakly on frequency. The numerical results for $\Sigma^{2p2p}(\omega)$, $B^{1s2p}(\omega)$, $g^{1s}(\omega)$ are shown in figure 3 and the corresponding parameters are given in table 1. The asymmetry factor $A2^{2p}(\omega) \simeq 0.4i \simeq 4B^{1s2p}(\omega)$ in the relevant energy region near the 2p resonance was taken from Shindo *et al* [33].

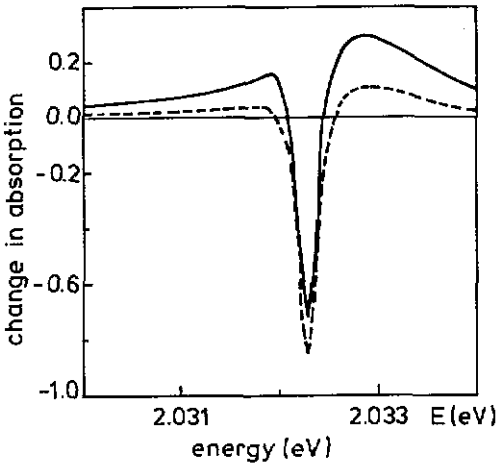

Figure 5. Comparison between difference spectra with (solid line) and without (dashed line) the sum frequency process. Parameters are the same as used in figure 4.

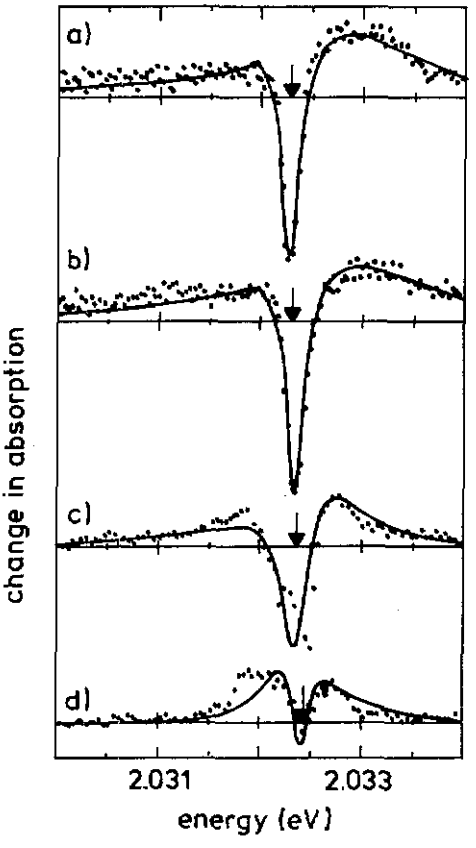

Figure 6. Dependence of differential transmission on pump energy $\hbar\omega_p$ and coupling strength $|V|^2 := |m^{1s2p}|^2 |E^p(0, \omega_p)|^2$. The dots represent the experimental results and the solid lines are theoretical spectra. The arrows indicate energy values of the measured spectral position of the 1s exciton in the linear spectra. Parameters used are: (a) $\hbar\omega_p = 116.8$ meV, $V = 2.8$ meV; (b) $\hbar\omega_p = 116.4$ meV, $V = 2.9$ meV; (c) $\hbar\omega_p = 115.9$ meV, $V = 2.0$ meV; (d) $\hbar\omega_p = 115.4$ meV, $V = 1.0$ meV. The fitted values for V are in excellent agreement with experimental results.

5. Results: comparison between theory and experiment

Figure 4 compares typically experimental transmission data with theoretical results. The asymmetric line shape of the linear spectrum T_0 is in fair agreement with the fitted curve. Our fit of the non-linear spectrum takes into account the attenuation of the CO_2 laser through the sample of thickness about 3 mm. The influence of the sum frequency generation is demonstrated in figure 5. In order to prove that the dynamical 1s–2p coupling is responsible for the difference spectrum in figure 4, Fröhlich *et al* [16] tuned the frequency ω_p and the intensity of the CO_2 laser. The experimental results, in comparison with our calculations, are shown in figure 6. The asymmetry of the line shapes is mainly induced by the vertex corrections of the envelope and interband dipole matrix elements.

Acknowledgments

We acknowledge useful discussions with Professor D Fröhlich (Universität Dortmund), Dr R Zimmermann (Zentralinstitut für Elektronenphysik, Berlin), R Scholz (RWTH Aachen), V M Axt (RWTH Aachen) and the financial support of this project by the Deutsche Forschungsgemeinschaft.

References

[1] Fröhlich D, Nöthe A and Reimann K 1985 *Phys. Rev. Lett.* **55** 1335
[2] Mysyrowicz A, Hulin D, Antonetti A, Migus A, Masselink W T and Morcoc H 1986 *Phys. Rev. Lett.* **56** 274
[3] Von Lehmen A, Chemla D S, Zucker J E and Heritage J P 1986 *Opt. Lett.* **11** 609
[4] Joffre M, Hulin D, Migus A and Combescot M 1989 *Phys. Rev. Lett.* **62** 74
[5] Wherret B S, Smirl A L and Bogess T F 1983 *IEEE J. Quantum Electron.* **QE-4** 680
[6] Huhn W and Stahl A 1984 *Phys. Status Solidi* b **124** 167
[7] Schmitt-Rink S and Chemla D S 1986 *Phys. Rev. Lett.* **57** 2752
[8] Stahl A and Balslev I 1987 *Electrodynamics of the Semiconductor Band Edge* (Berlin: Springer)
[9] Stahl A 1988 *Z. Phys.* B **72** 371
[10] Schlösser J and Stahl A 1989 *Phys. Status Solidi* b **153** 773
[11] Schmitt-Rink S, Chemla D S and Haug H 1988 *Phys. Rev.* B **37** 941
[12] Zimmermann R 1990 The dynamical Stark effect of excitons *Festkörperprobleme (Advances in Solid State Physics 30)* (Braunschweig: Vieweg) p 295
[13] Balslev I, Zimmermann R and Stahl A 1989 *Phys. Rev.* B **40** 4095
[14] Schlösser J, Stahl A and Balslev I 1990 *J. Phys. C: Solid State Phys.* **2** 5979
[15] Fröhlich D, Wille R, Schlapp W and Weimann G 1987 *Phys. Rev. Lett.* **59** 1748
[16] Fröhlich D, Neumann Ch, Uebbing B and Wille R 1990 *Phys. Status Solidi* b **159** 297
[17] Neumann Ch 1990 Untersuchungen des quadrupolaren Stark-Effekts in Cu_2O und des Intraband Stark-Effekts in MQW's *Thesis* Universität Dortmund
[18] Zimmermann R 1988 *Phys. Status Solidi* b **146** 545
[19] Toyozawa Y 1962 *Prog. Theor. Phys.* **27** 89
[20] Toyozawa Y 1964 *J. Phys. Chem. Solids* **25** 59
[21] Segall B 1967 *Phys. Rev.* **163** 769
[22] Segall B and Mahan G D 1968 *Phys. Rev.* **171** 935
[23] Rudin S and Reineke T L 1988 *Solid State Commun.* **68** 739
[24] Rudin S and Reineke T L 1989 *Phys. Rev.* B **39** 8488
[25] Zimmermann R 1990 *Phys. Status Solidi* b **159** 317
[26] Zimmermann R and Hartmann M 1990 *J. Cryst. Growth* **101** 341

[27] Haug H, Banyai L, Liebler J and Wicht T 1990 *Phys. Status Solidi* b **159** 309
[28] Agekyan V T 1977 *Phys. Status Solidi* a **43** 11
[29] Bufler F and Schlösser J 1991 *Phys. Rev.* B at press
[30] Elliott R J and Loudon R 1959 *J. Phys. Chem. Solids* **8** 382
[31] Stahl A and Frank D 1987 *Phys. Status Solidi* b **140** 301
[32] Elliott R J 1961 *Phys. Rev.* **124** 340
[33] Shindo K, Goto T and Anzai T 1974 *J. Phys. Soc. Japan* **36** 753
[34] Toyozawa Y 1972 *Polarons in Ionic Crystals and Polar Semiconductors* ed J T Devreese (Amsterdam: North-Holland) pp 1–27
[35] Schlösser J 1991 Zur nichtlinearen Optik von Exzitonen in Halbleitern *Thesis* RWTH Aachen
[36] Higashimura T, Iida T and Komatsu T 1988 *Phys. Status Solidi* b **150** 431
[37] Koster G F, Dimmock J O, Wheeler R G and Statz H 1963 *Proerties of the Thiry-Two Point Groups* (Cambridge, MA: MIT)
[38] Bloembergen N 1965 *Nonlinear Optics* (New York: Benjamin)
[39] Shen Y R 1984 *The Principles of Nonliner Optics* (New York: Wiley)
[40] *Landolt-Börnstein New Series* 1983 Group III, vol 17e (Berlin: Springer)
[41] Reimann K 1987 Dynamischer Stark-Effekt und Exziton-Relaxation in Cu_2O *Thesis* Universität Dortmund
[42] Weichman F L 1973 *Can. J. Phys.* **51** 680